these recall Ags in the presence of autologous monocytes (2.5×10^4 cells/well) that were previously isolated using autoMACS with anti-CD14 Ab (Miltenyi Biotec) and irradiated with x-ray at 30 Gy. The culture medium used for this assay was RPMI 1640 supplemented with 10% human serum. For proliferative responses to anti-CD3 mAb, total $CD4^+$ T cells or sorted subset T cells were stimulated with various concentrations of soluble CD3 (OKT-3) mAb (0.0001–1 μg/ml) in the presence of autologous monocytes. The culture medium used for this assay was RPMI 1640 medium supplemented with 10% FCS.

The effects of CD43 (0.05–5 μg/ml) and CD28 mAbs (1 μg/ml) on cell proliferation were evaluated. Proliferation was measured on day 3 for CD3 mAb and on day 5 for PPD by adding [^{3}H]thymidine (NEN, Boston, MA) at 1 μCi/well during the last 16 h of culture. All cultures were set up in triplicate.

Immunoprecipitation

Cells used for immunoprecipitation were KG-1 cells, PBMCs, MACS-purified $CD14^+$ monocytes, PBMCs depleted with $CD14^+$ monocytes, MACS-purified $CD4^+$ T cells, and activated $CD4^+$ T cells. Cells (5×10^6-1×10^7) were labeled at the cell surface by lactoperoxidase-catalyzed iodination as described previously (38). Radioiodinated cells were lysed with extraction buffer (0.5% Nonidet P-40, 10 mM Tris-HCl, 0.15 M NaCl, 1 mM PMSF, and 0.02% NaN_3) for 10 min on ice. The mixture was centrifuged at $27,000 \times g$ at 4°C for 20 min, and the supernatant was collected. Immunoprecipitations were performed by incubating radiolabeled cell lysate with 10 μg of HSCA-2, DFT-1, or MOPC21 mAbs for 1 h on ice, then adding a 20 μl-packed volume of protein G-Sepharose (Amersham Pharmacia Biotech, Piscataway, NJ), and further incubating the mixture for 30 min. Immunoprecipitates were washed four times in extraction buffer and solubilized in reducing Laemmli sample buffer subjected to SDS-PAGE (7.5% gel). After fixing and drying, the gels were autoradiographed at −80°C using x-ray film. Prestained SDS-PAGE standards were obtained from Bio-Rad (Hercules, CA).

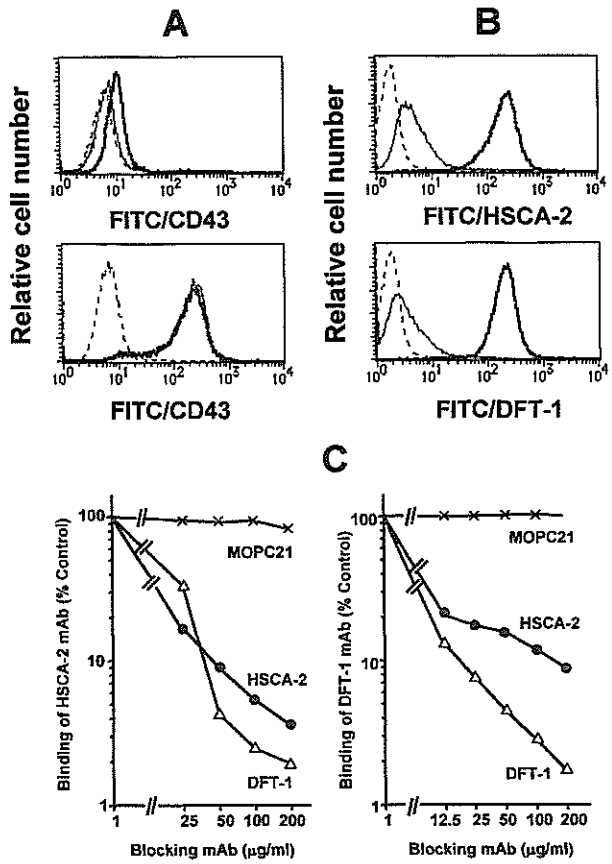

FIGURE 1. Flow cytometric analyses of CD43 expression in $CD43^+$ HeLa transfectant and KG-1 cells with HSCA-2 and DFT-1 mAbs. *A*, Direct immunofluorescence staining of mock-transfected (*upper panel*) and CD43-transfected HeLa cells (*lower panel*) with FITC-labeled HSCA-2 (thick line), DFT-1 (thin line), and control IgG1 (broken line) mAbs. *B*, Effect of neuraminidase treatment on the expression of CD43 in KG-1 cells. Nontreated (thick line) and treated (thin line) KG-1 cells were stained with FITC-labeled HSCA-2 (*upper panel*), DFT-1 (*lower panel*) mAbs. Treated cells also were stained with control IgG1 (broken line). *C*, Blocking of the binding of FITC-labeled HSCA-2 (*left*) and DFT-1 (*right*) mAbs to KG-1 cells by excess amounts of HSCA-2, DFT-1, or MOPC21 (IgG1 control) mAbs.

Results

Characterization of CD43 epitopes recognized by HSCA-2 mAb

HSCA-2 mAb resembles the reference CD43 mAb DFT-1 in binding to HeLa cells stably transfected with $CD43^+$ cDNA, but not to their mock-transfected ($CD43^-$) counterparts (Fig. 1*A*). HSCA-2 mAb also resembles the DFT-1 mAb in recognizing a neuraminidase-sensitive epitope on KG-1 cells (Fig. 1*B*). However, although the binding of HSCA-2 mAb to KG-1 cells was all but completely blocked by DFT-1 mAb, the binding of DFT-1 mAb was only ~90% blocked by HSCA-2 mAb even at the highest HSCA-2 mAb concentration (Fig. 1*C*). These findings may imply that the binding affinity of HSCA-2 mAb is lower than that of DFT-1 mAb. The HSCA-2 mAb immunoprecipitated a surface protein of ~115 kDa in KG-1 cells, whereas DFT-1 mAb immunoprecipitated both the115-kDa protein and a minor protein with a higher molecular mass of ~125 kDa (Fig. 2*A*). Immunoprecipitation and blocking experiments with another characterized CD43 mAb, 1G10, confirmed the results with the DFT-1 mAb (data not shown). These results suggest that HSCA-2 mAb reacts with a

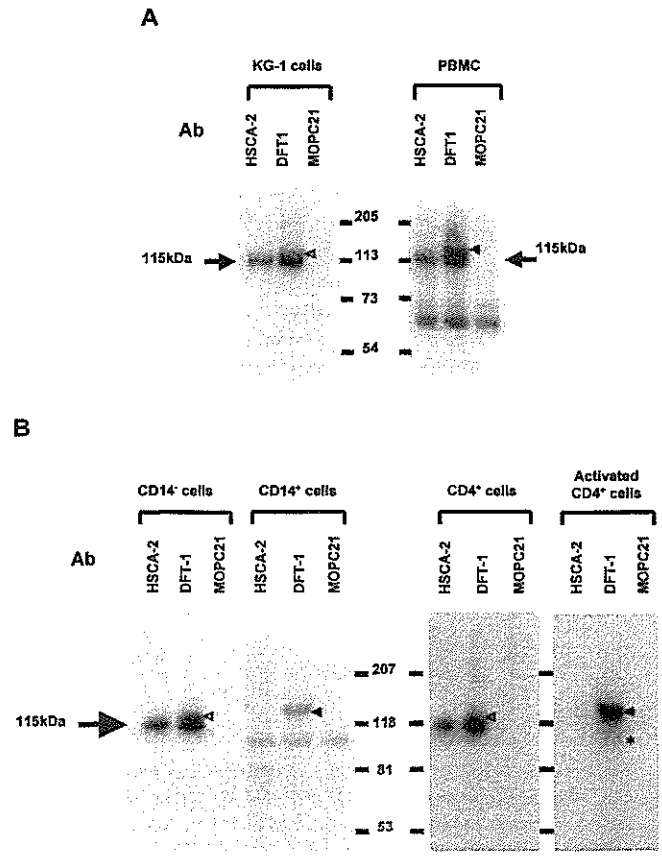

FIGURE 2. Immunoprecipitation of ^{125}I-labeled surface proteins from various types of white blood cells with HSCA-2, DFT-1, and MOPC21 (IgG1 control) mAbs. *A*, Immunoprecipitation of KG-1 cells and total PBMCs. *B*, Immunoprecipitation of $CD14^-$, $CD14^+$, $CD4^+$, and activated $CD4^+$ cells; 105-, 115-, 125-, and 135-kDa protein bands are indicated by an asterisk, arrows, open triangles, and closed triangles, respectively.

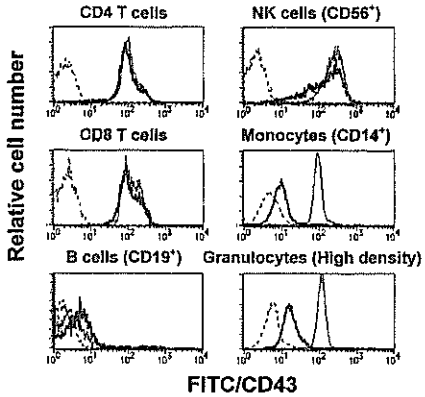

FIGURE 3. Flow cytometric analyses of CD43 expression in peripheral blood cells. For two-color analyses, PBMCs were stained with FITC-labeled HSCA-2 (thick line), DFT-1 (thin line), and control IgG1 (broken line) mAbs in combination with PE-labeled CD4, CD8, CD19, and CD56 mAbs. Monocytes and granulocytes isolated by MACS with CD14 mAb and density centrifugation, respectively, were singly stained with FITC-labeled mAbs. Results are representative of seven different donors.

sialic acid-dependent epitope on the 115-kDa CD43 glycoform in KG-1 cells, but not with its equivalent on the 125-kDa glycoform.

Expression characteristics of CD43 in normal white blood cells

The particular CD43 epitopes recognized by the HSCA-2 or DFT-1 mAb (hereafter abbreviated to CD43(HSCA-2) or CD43(DFT-1)) in normal lymphoid and myeloid cell populations were analyzed by two-color flow cytometry (Fig. 3). The CD43(HSCA-2) and CD43(DFT-1) epitopes were expressed at similar levels in $CD4^+$ and $CD8^+$ T cell populations. Neither HSCA-2 mAb nor DFT-1 mAb reacted with resting $CD19^+$ B cells, whereas they both bound reasonably strongly to either PWM-activated or EBV-transformed B cells (data not shown). The majority of $CD56^+$ NK cells expressed both CD43(HSCA-2) and CD43(DFT-1) epitopes at high levels, whereas there was relatively little of the CD43(HSCA-2) epitope in the minor subpopulation of NK cells. DFT-1 mAb was found to bind quite strongly to both purified monocytes and granulocytes, whereas binding by the HSCA-2 mAb was weak enough to be described as nonspecific, as judged by the results of immunoprecipitation analyses (see Fig. 2*B*). We did not detect any increase in the level of either CD43(HSCA-2) or CD43(DFT-1) in cultured monocytes, even after the addition of LPS (data not shown). The HSCA-2 and DFT-1 mAbs both reacted quite strongly with cord blood $CD34^+$ cells (data not shown). Two previously used CD43 mAbs, 1G10 and L10, appeared to share the cell type specificities of the DFT-1 mAb (data not shown).

The results of experiments involving immunoprecipitation of ^{125}I-labeled surface proteins from PBMCs, $CD14^-$ lymphoid cells, and $CD4^+$ T cells with CD43 mAbs revealed that the HSCA-2 mAb recognizes only 115-kDa proteins, and whereas the DFT-1 mAb also reacts with 115-kDa proteins it can interact with a second minor, but higher molecular mass (~125 kDa), protein as well (Fig. 2); these findings mirror our previous findings with KG-1 cells (see above). Other findings include the fact that HSCA-2 mAb failed to immunoprecipitate any specific proteins from $CD14^+$ monocytes, unlike the DFT-1 mAb, which reacted with a 135-kDa protein (Fig. 2*B*). In tests with activated $CD4^+$ T cells, the DFT-1 mAb immunoprecipitated both the 135-kDa protein and a minor protein with lower molecular mass of 105 kDa, unlike the HSCA-2 mAb, which did not react with proteins of either of these sizes (Fig. 2*B*). Both the HSCA-2 and DFT-1 mAbs appeared to specifically immunoprecipitate several common, low molecular mass (25- to 40-kDa) proteins in activated $CD4^+$ T cells (data not shown).

Expression characteristics of CD43 in $CD4^+$ memory T cells

As shown in Fig. 4 (*left*), the $CD4^+CD45RO^+$ cell population can be divided into three distinct subsets (M1, M2, and M3) on the basis of their CD43(HSCA-2) expression levels; this confirms our previous findings (31). We therefore tried to define the same three subsets on the basis of their CD43(DFT-1) expression levels (Fig. 4, *right*); interestingly, the proportions of the M1 subset detected with the DFT-1 and HSCA-2 mAbs were not significantly different (Table I), whereas the proportion of the M2 subset defined by the DFT-1 mAb was significantly larger when defined by HSCA-2 mAb, and the proportion of the M3 subset defined by the DFT-1 mAb was significantly smaller than when defined by HSCA-2 mAb. We observed similar subset percentages when the 1G10 and L10 mAbs were used in place of the DFT-1 mAb (Table I). These results indicate that the low levels of CD43(HSCA-2) expression that typify the M3 population do not affect the ability of M3 cells to express other CD43 epitopes.

Accessory functions of CD43 in recall responses of $CD4^+$ memory T cells

To analyze possible accessory functions of CD43(HSCA-2) in memory T cells, we first examined the effects of exposure to HSCA-2 mAb on the recall Ag-induced proliferation of total PBMCs in culture. As shown in Fig. 5, HSCA-2 mAb seemed to

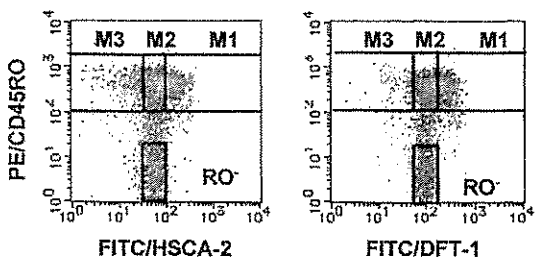

FIGURE 4. Flow cytometric analyses of CD43 expression in $CD4^+$ T cell subsets. Expression of CD43 detected by either HSCA-2 (*left*) or DFT-1 (*right*) mAbs in combination with CD45RO in $CD4^+$ T cells analyzed by triple-color immunofluorescence. Four different subsets were defined within $CD4^+$T cells: $CD45RO^+$ cells expressing higher (M1), intermediate (M2), and lower (M3) levels of CD43, and $CD45RO^-$ (RO^-) cells in each CD43 mAb. In each donor a window for the M2 subset was set in a region where the CD43 level detected by each CD43 mAb was from approximately one-half to 2-fold the mean CD43 intensity for RO^- cells. Results are representative of six donors.

Table I. *CD4 memory T cell subsets defined by four different CD43 mAbs*

CD43 mAb	Subsets (% in total $CD4^+$ T cells[a])		
	M1	M2	M3
HSCA-2	19.9 ± 4.4[b]	21.8 ± 8.0	5.7 ± 3.0
DFT-1	19.0 ± 3.7	25.3 ± 9.4[c]	3.0 ± 1.4[c]
L10	20.5 ± 4.3	23.6 ± 8.7[c]	2.6 ± 1.4[c]
1G10	19.0 ± 4.1	24.5 ± 8.2[c]	2.8 ± 1.8[c]

[a] The percentage of each subset in total $CD4^+$ T cells was determined by three-color flow cytometry, as shown in Fig. 4*A*.
[b] Average ± SD (n = 6)
[c] Value was significantly larger or smaller than that of HSCA-2 mAb by Wilcoxon signed rank test ($p < 0.05$).

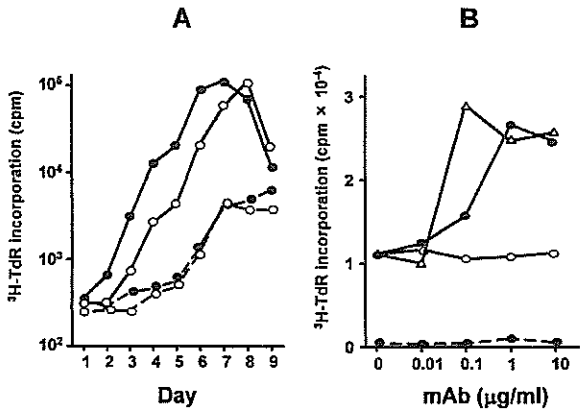

FIGURE 5. Acceleration of proliferative responses of PBMCs to PPD by stimulation with CD43 mAbs. *A*, Time courses of PPD responses. PBMCs were stimulated with (solid line) or without (broken line) PPD (5 μg/ml) in the presence (●) or the absence (○) of HSCA-2 mAb (5 μg/ml). *B*, Dose responses of CD43 mAbs. PBMCs were stimulated with (solid line) or without (broken line) PPD (5 μg/ml) in the presence of HSCA-2 (●), DFT-1 (△), and MOPC21 (○) at the various concentrations. Proliferation was measured on day 5 by adding [^{3}H]thymidine during the last 16 h of culture. Results are representative of five donors.

dose-dependently accelerate the proliferation of PPD Ag-stimulated PBMCs, but had no comparable effect on their proliferation in the absence of PPD. The three traditionally used anti-CD43 mAbs (DFT-1 (Fig. 5*B*), and 1G10 and L10 (data not shown)) also proved at least as effective as the HSCA-2 mAb in accelerating PPD-stimulated proliferation of PBMCs. As the majority of PPD-reactive cells appear to be CD4+ T cells (data not shown), we examined the effects of the addition of a combination of HSCA-2 mAb and CD28 mAb on the responses of MACS-purified CD4+ T cells in the presence of autologous monocytes (Fig. 6). The CD28 mAb that we chose to use in this experiment was the CD28.2 clone, which is capable of strongly costimulating polyclonal T cell responses to plastic- or monocyte-bound CD3 mAb, but (if anything) inhibits Ag-specific responses (39). Thus, whereas HSCA-2 mAb led to a significantly enhanced PPD response in CD4+ T cells, the addition of CD28 mAb led to it being slightly inhibited. We also examined the effect of the HSCA-2 mAb on the TT-dependent proliferative response of CD4+ T cells and found that it had an enhancing effect (Fig. 6).

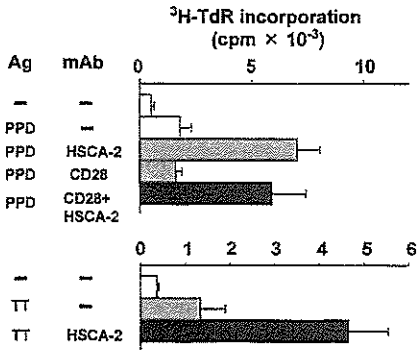

FIGURE 6. Effects of HSCA-2 and CD28 mAbs on the proliferative responses of CD4 T cells to recall Ags. MACS-purified CD4 T cells were stimulated with PPD or TT in the presence of autologous CD14+ APC. HSCA-2 (5 μg/ml) and/or CD28 (1 μg/ml) mAbs were added to the culture. Proliferation was measured on day 5 (PPD) or day 7 (TT) by adding [^{3}H]thymidine during the last 16 h of culture. Results were expressed as the mean cpm ± SD and are representative of three donors.

Next we examined the effects of the addition of CD28 and HSCA-2 mAbs on recall responses in each of the three CD4+ memory T cell subsets as defined by their separation in a cell sorter on the basis of their CD43(HSCA-2) expression levels (Fig. 4). As shown in Fig. 7*A*, only the M1 subset cells appeared to be capable of responding to PPD; this confirms our previous findings (31). The results of our experiments with the M1 subset mirrored our findings with unseparated CD4+ T cell populations, in that the PPD response of M1 subset cells was significantly and dose-dependently enhanced by the addition of HSCA-2 mAb (Fig. 7, *B* and *C*), but was inhibited, rather than enhanced, in the presence of the CD28 mAb (Fig. 7*A*). The PPD responses of the M2 and M3 subset cells were virtually unaffected by the addition of the HSCA-2 mAb (Fig. 7, *B* and *C*). This did not surprise us, given that the M2 and M3 subsets appeared to contain a relatively very

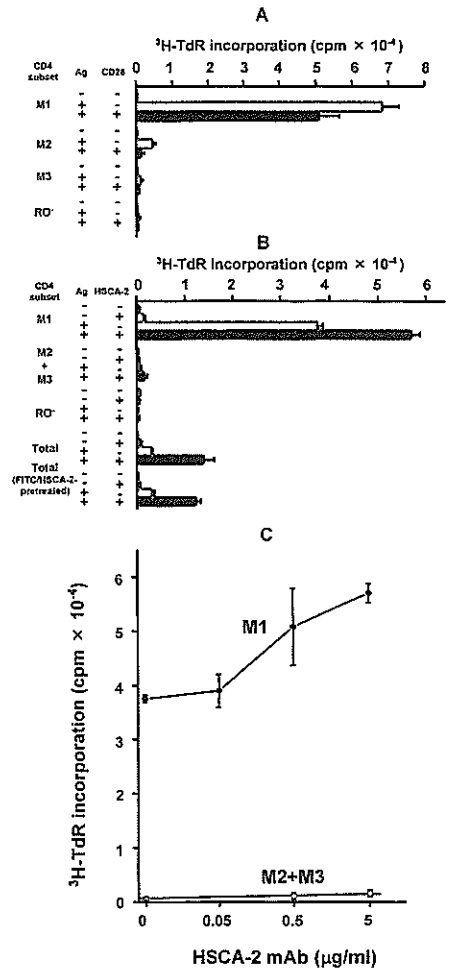

FIGURE 7. Effects of CD28 and HSCA-2 mAbs on the proliferative responses of CD4 T cell subsets to PPD. *A–C*, MACS-purified CD4+ T cells were stained with FITC-HSCA-2 and PE-CD45RO mAbs (see Fig. 4*A*, *left*) and thereafter sorted by FACS into the indicated subsets. Each subset cells and total CD4+ T cells were stimulated with PPD in the presence of autologous CD14+ APC. CD28 (1 μg/ml; *A*) or HSCA-2 (5 μg/ml; *B*) mAbs were added to the culture. Total CD4+ T cells pretreated with FITC-HSCA-2 mAb also were examined for possible effects of immunofluorescence staining with HSCA-2 mAb on the PPD response (*B*). M2+M3, Cell populations sorted by gating the combined region of the M2 and M3 subsets (Fig. 4*A*, *left*). Dose responses of HSCA-2 mAb for M1 subset cells and a combined cell population of M2 and M3 subsets were examined (*C*). Proliferation was measured on day 5 by adding [^{3}H]thymidine during the last 16 h of culture. Results were expressed as the mean cpm ± SD and are representative of three donors.

small PPD-reactive precursor component (31). The stimulatory effect of the FITC-HSCA-2 mAb that remains attached to cells after its use in the course of their separation was negligible, given that the pretreatment of unseparated CD4$^+$ T cells with FITC-HSCA-2 mAb did not significantly alter their subsequent response to PPD, whereas addition of the mAb to cultures of both FITC-HSCA-2 mAb-pretreated and nontreated CD4$^+$ T cells increased their responses to PPD to very much the same extent (Fig. 7*B*). Taken together, the above results indicate that CD43(HSCA-2) is capable of acting as an accessory molecule in the Ag-specific recall response of mature CD4$^+$ memory T cells.

Synergistic effects between CD43 and CD28 mAbs in polyclonal response

To determine whether CD43(HSCA-2) can play an accessory role in the polyclonal activation of T cells, we examined the possible effects of the HSCA-2 mAb on the proliferative response of CD4$^+$ T cells to monocyte-bound CD3 mAb (Fig. 8). We found that the HSCA-2 mAb did have an effect, but that it was only marginally costimulatory at lower (0.001–0.1 μg/ml) CD3 mAb concentrations and that its effectiveness disappeared at the highest concentration tested (1 μg/ml). Interestingly, the results shown in Fig. 8*A* provide convincing evidence that the CD28/HSCA-2 mAb combination had a synergistic effect on the CD3 mAb-mediated polyclonal response (Fig. 8*A*). A similar synergistic effect on the CD3-mediated response was observed when the mAbs involved were DFT-1 and CD28 (data not shown).

Cells of two of the three CD4$^+$ memory T cell subsets (M1 and M2) responded strongly to monocyte-bound CD3 mAb, whereas M3 subset cells did not (Fig. 8*B*). These findings are in agreement with those in our original report (31). The HSCA-2 mAb was almost as effective as CD28 mAb in their enhancement of polyclonal responses in M1 and M2 subset cells, but had no such effect in M3 subset cells. There were marginal synergistic effects on polyclonal responses when M1 and M2 subset cells were cotreated with the HSCA-2 and CD28 mAbs, although a much more obvious synergistic effect became evident when we used RO$^-$ naive subset cells instead.

When the Fab portion of the HSCA-2 mAb was used instead of intact Ab, we could see no indication of either an enhanced PPD-mediated stimulatory response or a synergistic interaction involving the CD28 mAb and CD3 mAb polyclonal responses (data not shown).

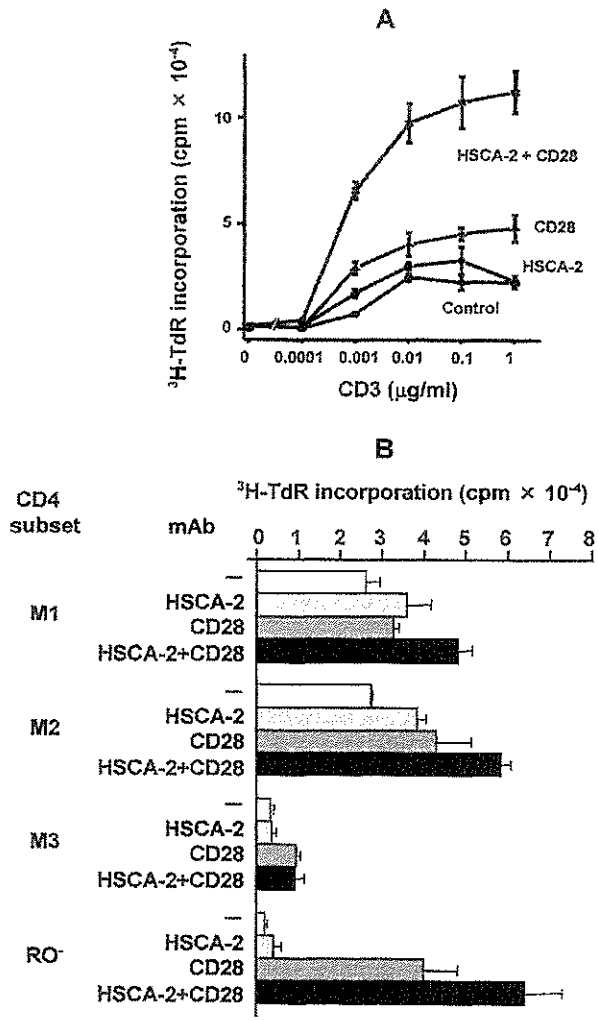

FIGURE 8. Synergistic effects of HSCA-2 and CD28 mAbs on the proliferative responses of CD4$^+$ T cells to monocyte-bound CD3 mAb. Total CD4$^+$ T cells (*A*) and CD4$^+$ T cell subset cells (*B*) were stimulated with various concentrations (*A*) or 0.1 μg/ml (*B*) of CD3 mAb in the presence of autologous CD14$^+$ monocytes. The effects of HSCA-2 (5 μg/ml) and CD28 (1 μg/ml) mAbs on the CD3 responses were tested by single or combined use of these mAbs. Proliferation was measured on day 3 by adding [^{3}H]thymidine during the last 16 h of culture. Results were expressed as the mean cpm ± SD and are representative of three donors.

Discussion

HSCA-2 mAb specifically recognizes a neuraminidase-sensitive epitope on the low molecular mass (115-kDa) glycoform of the CD43 molecule that is predominantly expressed in lymphoid cells, including resting T and NK cells. By contrast, all previously described CD43 mAbs (including the DFT-1 mAb) react strongly or even very strongly with a larger (135-kDa) CD43 glycoform that is expressed in myeloid cells such as monocytes and granulocytes. Importantly, the HSCA-2 mAb does not appear to recognize the 135-kDa glycoform and hence binds only marginally, if at all, to myeloid cells; it also does not immunoprecipitate a third high molecular mass (125-kDa) CD43 protein that is recognized by the DFT-1mAb in both KG-1 and CD4$^+$ T cells. Taken together, these findings suggest that the HSCA-2 mAb is specific for a novel glycoepitope on the 115-kDa glycoform of CD43.

Interestingly, HSCA-2 mAb differs from all pre-existing CD43 mAbs in being unable to recognize the high molecular mass CD43 glycoform (135 kDa) that is present on activated CD4$^+$ T cells. Thus, the 135-kDa CD43 glycoform consists of a more fully glycosylated version that is generated in the course of the increase in molecular mass of the 115-kDa CD43 glycoform that occurs during T cell activation (5, 7); it is possible that the HSCA-2 glycoepitope is either lost or masked in the course of this glycosyl modification process. As the molecular mass of the CD43 polypeptide is ~40 kDa, the 25- to 40-kDa proteins recognized by HSCA-2 mAb in activated T cells could well be degradation forms of CD43, and we have even observed what appeared to be the gradual disappearance of CD43(HSCA-2) epitopes from a subpopulation of activated CD4$^+$CD45RO$^+$ T cells (manuscript in preparation).

We noticed that there were significant differences in the distribution of the CD4 memory T cell subsets depending upon which of the available CD43 mAbs was used in their separation. Thus, for example, the percentages of M2 subset cells that we observed in separations achieved using the HSCA-2 mAb were significantly smaller than those observed in separations using any of the other available mAbs. In the case of the M3 subsets, the percentages were larger with the HSCA-2 mAb than with any of the others. These CD43 mAb-dependent differences in subset distributions

may correspond to differences in such subset cell functions as memory vs anergy, but we have yet to explore this possibility in any detail.

In this report we show that HSCA-2 and certain other CD43 mAbs are capable of accelerating both the recall Ag-induced and CD3 mAb-induced proliferation of CD4 memory T cells. There are previous reports indicating that CD43 molecules may also have accessory involvements in T cell activation, such as, for example, in mice, where CD43 mAb appears to costimulate T cell activation during treatment with plastic-bound CD3 mAb and alloantigens (17, 40). In humans, however, there does not appear to be any evidence of CD43 mAb being involved in a costimulatory capacity in the polyclonal activation of T cells (41). In situations involving Ag-specific responses, there is one report that CD43 is necessary for the production of IL-2 in HLA class II-specific human hybridoma T cells (42), but it is important to note that the experimental system used to obtain these data was an unusually artificial one. There are, however, several publications in which it is claimed that a number of CD43 mAbs can stimulate Ag-independent human T cell proliferation in a multicomponent test system that requires the presence of CD43-stimulated monocytes (43–46). Thus, the results described in this study appear to provide the first evidence that T cell-determined CD43 may help to stimulate the Ag-specific proliferative responses of freshly isolated T cells in humans. In the case of our new mAb (HSCA-2), we can exclude any involvement of CD43-mediated monocyte stimulation in T cell activation. The reason why HSCA-2 mAb differs from all previously used CD43 mAbs in this important way is that it appears to lack reactivity to the 135-kDa CD43 glycoform expressed in monocytes.

Given the above consideration, it seems reasonable to assume that CD43 plays a part in some of the cell signaling events that are likely to be involved in memory T cell activation. Up-regulated expression of CD43 in M1 subset cells may cause an increase in activation signaling in concert with other up-regulated costimulatory molecules such as CD28 (31). Our observation that CD43 and CD28 mAbs act synergistically to stimulate the polyclonal response of CD4$^+$ T cells to anti-CD3 mAb may indicate that both CD43 and CD28 have an accessory signaling role in the induction of the polyclonal response. It has previously been reported that T cell activation through CD43 cross-linking in humans induces serine phosphorylation of Cbl proteins and tyrosine phosphorylation of Vav (19, 20). It has also been reported that one of the CD28-determined costimulatory signaling processes is mediated by tyrosine phosphorylation of Vav1, which is, in turn, negatively regulated by Cbl-b (47–49). Thus, although the precise molecular mechanisms underlying the costimulatory effects of CD43 remain to be determined, it is possible that both CD28 and CD43 are capable of synergistically enhancing the activation of CD4$^+$ memory T cells by a mechanism involving the common signaling pathway.

Acknowledgments

We grateful to Dr. Donald MacPhee for his valuable suggestions, to Mika Yamaoka for her excellent assistance with FACS analysis, and to Mika Yonezawa and Jeffrey Hart for manuscript preparation.

References

1. Remold-O'Donnell, E. 1995. CD43 cluster report. In *Leucocyte Typing*. Vol. V: *White Cell Differentiation Antigens*. S. F. Schlossman, L. Boumsell, W. Gilks, J. M. Harlan, T. Kishimoto, C. Morimoto, J. Ritz, S. Shaw, R. Silverstein, T. Springer, et al., eds. Oxford University Press, New York, p. 1697.
2. Rosenstein, Y., A. Santana, and G. Pedraza-Alva. 1999. CD43, a molecule with multiple functions. *Immunol. Res. 20:89.*
3. Cyster, J. G., D. M. Shotton, and A. F. Williams. 1991. The dimensions of the T lymphocyte glycoprotein leukosialin and identification of linear protein epitopes that can be modified by glycosylation. *EMBO J. 10:893.*
4. Carlsson, S. R., H. Sasaki, and M. Fukuda. 1986. Structural variations of *O*-linked oligosaccharides present in leukosialin isolated from erythroid, myeloid, and T-lymphoid cell lines. *J. Biol. Chem. 261:12787.*
5. Piller, F., F. Le Deist, K. I. Weinberg, R. Parkman, and M. Fukuda. 1991. Altered *O*-glycan synthesis in lymphocytes from patients with Wiskott-Aldrich syndrome. *J. Exp. Med. 173:1501.*
6. Jones, A. T., B. Federsppiel, L. G. Ellies, M. J. Williams, R. Burgener, V. Duronio, C. A. Smith, F. Takei, and H. J. Ziltener. 1994. Characterization of the activation-associated isoform of CD43 on murine T lymphocytes. *J. Immunol. 153:3426.*
7. Piller, F., V. Piller, R. I. Fox, and M. Fukuda. 1988. Human T-lymphocyte activation is associated with changes in *O*-glycan biosynthesis. *J. Biol. Chem. 263:15146.*
8. Harrington, L. E., M. Galvan, L. G. Baum, J. D. Altman, and R. Ahmed. 2000. Differentiating between memory and effector CD8 T cells by altered expression of cell surface *O*-glycans. *J. Exp. Med. 191:1241.*
9. Onami, T. M., L. E. Harrington, M. A. Williams, M. Galvan, C. P. Larsen, T. C. Pearson, N. Manjunath, L. G. Baum, B. D. Pearce, and R. Ahmed. 2002. Dynamic regulation of T cell immunity by CD43. *J. Immunol. 168:6022.*
10. Ostberg, J. R., R. K. Barth, and J. G. Frelinger. 1998. The Roman god Janus: a paradigm for the function of CD43. *Immunol. Today 19:546.*
11. Manjunath, N., M. Correa, M. Ardman, and B. Ardman. 1995. Negative regulation of T-cell adhesion and activation by CD43. *Nature 377:535.*
12. Stockton, B. M., G. Cheng, N. Manjunath, B. Ardman, and U. H. von Andrian. 1998. Negative regulation of T cell homing by CD43. *Immunity 8:373.*
13. McEvoy, L. M., H. Sun, J. G. Frelinger, and E. C. Butcher. 1997. Anti-CD43 inhibition of T cell homing. *J. Exp. Med. 185:1493.*
14. Woodman, R. C., B. Johnston, M. J. Hickey, D. Teoh, P. Reinhardt, B. Y. Poon, and P. Kubes. 1998. The functional paradox of CD43 in leukocyte recruitment: a study using CD43-deficient mice. *J. Exp. Med. 188:2181.*
15. He, Y. W., and M. J. Bevan. 1999. High level expression of CD43 inhibits T cell receptor/CD3-mediated apoptosis. *J. Exp. Med. 190:1903.*
16. Brown, T. J., W. W. Shuford, W. C. Wang, S. G. Nadler, T. S. Bailey, H. Marquardt, and R. S. Mittler. 1996. Characterization of a CD43/leukosialin-mediated pathway for inducing apoptosis in human T-lymphoblastoid cells. *J. Biol. Chem. 271:27686.*
17. Sperling, A. I., J. M. Green, R. L. Mosley, P. L. Smith, R. J. DiPaolo, J. R. Klein, J. A. Bluestone, and C. B. Thompson. 1995. CD43 is a murine T cell costimulatory receptor that functions independently of CD28. *J. Exp. Med. 182:139.*
18. Pedraza-Alva, G., L. B. Merida, S. J. Burakoff, and Y. Rosenstein. 1996. CD43-specific activation of T cells induces association of CD43 to Fyn kinase. *J. Biol. Chem. 271:27564.*
19. Pedraza-Alva, G., L. B. Merida, S. J. Burakoff, and Y. Rosenstein. 1998. T cell activation through the CD43 molecule leads to Vav tyrosine phosphorylation and mitogen-activated protein kinase pathway activation. *J. Biol. Chem. 273:14218.*
20. Pedraza-Alva, G., S. Sawasdikosol, Y. C. Liu, L. B. Merida, M. E. Cruz-Munoz, F. Oceguera-Yanez, S. J. Burakoff, and Y. Rosenstein. 2001. Regulation of Cbl molecular interactions by the co-receptor molecule CD43 in human T cells. *J. Biol. Chem. 276:729.*
21. Thurman, E. C., J. Walker, S. Jayaraman, N. Manjunath, B. Ardman, and J. M. Green. 1998. Regulation of in vitro and in vivo T cell activation by CD43. *Int. Immunol. 10:691.*
22. Carlow, D. A., S. Y. Corbel, and H. J. Ziltener. 2001. Absence of CD43 fails to alter T cell development and responsiveness. *J. Immunol. 166:256.*
23. Allenspach, E. J., P. Cullinan, J. Tong, Q. Tang, A. G. Tesciuba, J. L. Cannon, S. M. Takahashi, R. Morgan, J. K. Burkhardt, and A. I. Sperling. 2001. ERM-dependent movement of CD43 defines a novel protein complex distal to the immunological synapse. *Immunity 15:739.*
24. Delon, J., K. Kaibuchi, and R. N. Germain. 2001. Exclusion of CD43 from the immunological synapse is mediated by phosphorylation-regulated relocation of the cytoskeletal adaptor moesin. *Immunity 15:691.*
25. Shaw, A. S. 2001. FERMing up the synapse. *Immunity 15:683.*
26. Stoll, S., J. Delon, T. M. Brotz, and R. N. Germain. 2002. Dynamic imaging of T cell-dendritic cell interactions in lymph nodes. *Science 296:1873.*
27. Cullinan, P., A. I. Sperling, and J. K. Burkhardt. 2002. The distal pole complex: a novel membrane domain distal to the immunological synapse. *Immunol. Rev. 189:111.*
28. Savage, N. D., S. L. Kimzey, S. K. Bromley, K. G. Johnson, M. L. Dustin, and J. M. Green. 2002. Polar redistribution of the sialoglycoprotein CD43: implications for T cell function. *J. Immunol. 168:3740.*
29. Youseffi-Etemad, R., and B. Axelsson. 1996. Parallel pattern of expression of CD43 and of LFA-1 on the CD45RA$^+$ (naive) and CD45RO$^+$ (memory) subsets of human CD4$^+$ and CD8$^+$ cells: correlation with the aggregative response of the cells to CD43 monoclonal antibodies. *Immunology 87:439.*
30. Mukasa, R., T. Homma, T. Ohtsuki, O. Hosono, A. Souta, T. Kitamura, M. Fukuda, S. Watanabe, and C. Morimoto. 1999. Core 2-containing *O*-glycans on CD43 are preferentially expressed in the memory subset of human CD4 T cells. *Int. Immunol. 11:259.*
31. Ohara, T., K. Koyama, Y. Kusunoki, T. Hayashi, N. Tsuyama, Y. Kubo, and S. Kyoizumi. 2002. Memory functions and death proneness in three CD4$^+$CD45RO$^+$ human T cell subsets. *J. Immunol. 169:39.*
32. Sallusto, F., D. Lenig, R. Forster, M. Lipp, and A. Lanzavecchia. 1999. Two subsets of memory T lymphocytes with distinct homing potentials and effector functions. *Nature 401:708.*
33. Kyoizumi, S., M. Akiyama, N. Kouno, K. Kobuke, M. Hakoda, S. L. Jones, and M. Yamakido. 1985. Monoclonal antibodies to human squamous cell carcinoma of the lung and their application to tumor diagnosis. *Cancer Res. 45:3274.*

34. Andrew, S. M., and J. Titus. 1996. Fragmentation of immunogloblin G. In *Current Protocols in Immunology*. J. E. Coligan, A. M. Kruisbeek, D. H. Margulies, E. M. Shevach, and W. Strober, eds. John Wiley & Sons, New York and London, p. 2. 10.
35. Nunes, J., S. Klasen, M. Ragueneau, C. Pavon, D. Couez, C. Mawas, M. Bagnasco, and D. Olive. 1993. CD28 mAbs with distinct binding properties differ in their ability to induce T cell activation: analysis of early and late activation events. *Int. Immunol. 5:311*.
36. Remold-O'Donnell, E., D. M. Kenney, R. Parkman, L. Cairns, B. Savage, and F. S. Rosen. 1984. Characterization of a human lymphocyte surface sialoglycoprotein that is defective in Wiskott-Aldrich syndrome. *J. Exp. Med. 159:1705*.
37. Horejsi, V., and H. Stockinger. 1997. CD43 workshop panel report. In *Leucocyte Typing*, Vol. VI: *White Cell Differentiation Antigens*. T. Kishimoto, H. Kikutani, A. E. G. Kr. von dem Borne, S. M. Goyert, D. Y. Mason, M. Miyasaka, L. Moretta, K. Okumura, S. Shaw, T. A. Springer, et al., eds. Garland, New York and London, p. 494.
38. Kyoizumi, S., M. Akiyama, Y. Hirai, Y. Kusunoki, K. Tanabe, and S. Umeki. 1990. Spontaneous loss and alteration of antigen receptor expression in mature $CD4^+$ T cells. *J. Exp. Med. 171:1981*.
39. Olive, D., C. Cerdan, R. Costello, I. Sielleur, M. Ragueneau, F. Pages, S. Klasen, J. Nunes, and J. Imbert. 1995. CD28 and CTLA-4 cluster report. In *Leucocyte Typing*, Vol. V: *White Cell Differentiation Antigens*. S. F. Schlossman, L. Boumsell, W. Gilks, J. M. Harlan, T. Kishimoto, C. Morimoto, J. Ritz, S. Shaw, R. Silverstein, T. Springer, et al., ed. Oxford University Press, New York, p. 360.
40. Walker, J., and J. M. Green. 1999. Structural requirements for CD43 function. *J. Immunol. 162:4109*.
41. Tkaczuk, J., T. Al Saati, I. Escargueil-Blanc, A. Salvayre, V. Horejsi, M. Durand, C. de Preval, E. Ohayon, G. Delsol, and M. Abbal. 1999. The CBF.78 monoclonal antibody to human sialophorin has distinct properties giving new insights into the CD43 marker and its activation pathway. *Tissue Antigens 54:1*.
42. Park, J. K., Y. J. Rosenstein, E. Remold-O'Donnell, B. E. Bierer, F. S. Rosen, and S. J. Burakoff. 1991. Enhancement of T-cell activation by the CD43 molecule whose expression is defective in Wiskott-Aldrich syndrome. *Nature 350:706*.
43. Mentzer, S. J., E. Remold-O'Donnell, M. A. Crimmins, B. E. Bierer, F. S. Rosen, and S. J. Burakoff. 1987. Sialophorin, a surface sialoglycoprotein defective in the Wiskott-Aldrich syndrome, is involved in human T lymphocyte proliferation. *J. Exp. Med. 165:1383*.
44. Axelsson, B., R. Youseffi-Etemad, S. Hammarstrom, and P. Perlmann. 1988. Induction of aggregation and enhancement of proliferation and IL-2 secretion in human T cells by antibodies to CD43. *J. Immunol. 141:2912*.
45. Nong, Y. H., E. Remold-O'Donnell, T. W. LeBien, and H. G. Remold. 1989. A monoclonal antibody to sialophorin (CD43) induces homotypic adhesion and activation of human monocytes. *J. Exp. Med. 170:259*.
46. Alvarado, M., C. Klassen, J. Cerny, V. Horejsi, and R. E. Schmidt. 1995. MEM-59 monoclonal antibody detects a CD43 epitope involved in lymphocyte activation. *Eur. J. Immunol. 25:1051*.
47. Chiang, Y. J., H. K. Kole, K. Brown, M. Naramura, S. Fukuhara, R. J. Hu, I. K. Jang, J. S. Gutkind, E. Shevach, and H. Gu. 2000. Cbl-b regulates the CD28 dependence of T-cell activation. *Nature 403:216*.
48. Bachmaier, K., C. Krawczyk, I. Kozieradzki, Y. Y. Kong, T. Sasaki, A. Oliveira-dos-Santos, S. Mariathasan, D. Bouchard, A. Wakeham, A. Itie, et al. 2000. Negative regulation of lymphocyte activation and autoimmunity by the molecular adaptor Cbl-b. *Nature 403:211*.
49. Krawczyk, C., K. Bachmaier, T. Sasaki, G. R. Jones, B. S. Snapper, D. Bouchard, I. Kozieradzki, S. P. Ohashi, W. F. Alt, and M. J. Penninger. 2000. Cbl-b is a negative regulator of receptor clustering and raft aggregation in T cells. *Immunity 13:463*.

19

Flow Cytometric Measurement of Mutant T Cells With Altered Expression of *TCR*

Detecting Somatic Mutations in Humans and Mice

Seishi Kyoizumi, Yoichiro Kusunoki, and Tomonori Hayashi

Summary

Spontaneously generated mutant T cells defective in T-cell receptor (*TCR*) gene expression are detectable at the frequency of 10^{-4} in vivo, and the mutant fractions are dose-dependently increased by exposure to genotoxic substances such as ionizing radiation. Mutant cells with altered expression of TCR-α or -β among $CD4^+$ T cells can be detected as $CD3^-/CD4^+$ cells by two-color flow cytometry using anti-CD3 and anti-CD4 monoclonal antibodies labeled with different fluorescent dyes, because an incomplete TCRαβ/CD3 complex cannot be transported to the cellular membrane. This flow cytometric mutation assay can be applied to $CD4^+$ T cells from human peripheral blood and mouse spleen. Methods for both preparation of target cells and detection of the mutant cells are described.

Key Words: Somatic mutation; flow cytometry; T-cell receptor (TCR), $CD4^+$ T cell; human peripheral blood; mouse spleen.

1. Introduction

Monitoring of somatic mutation in vivo is useful for evaluating cancer risk from exposure to environmental genotoxic substances, including ionizing radiation and chemicals. Assays of in vivo somatic mutations have been established for various target genes *(1)*. The flow cytometric T-cell receptor (*TCR*) mutation assay allows reproducible measurement of mutant fractions (Mfs) at the *TCR-α* (*TCRA*) and *TCR-β* (*TCRB*) genes of peripheral mature $CD4^+$ T cells in individual humans *(2)* and mice *(3)*.

The TCR-α and -β proteins are expressed on the cell surface of normal peripheral $CD4^-$ and $CD8^+$ T cells. In most of these T-cell populations, only one of the two alleles of each *TCR* chain gene is actively expressed, although it has been reported that a minor T-cell subpopulation coexpresses dual α or β chains *(4,5)*. The second allele of these loci remains unexpressed owing to nonfunctional recombination or epigenetic inactivation resulting in allelic exclusion *(6)*. Thus, mutants that do not express TCR can be

From: *Methods in Molecular Biology, vol. 291, Molecular Toxicology Protocols*
Edited by: P. Keohavong and S. G. Grant © Humana Press Inc., Totowa, NJ

generated in the majority of the T-cell population by a single inactivation event, even though the *TCR* genes are autosomally located. Further, TCR-α and β chains can be expressed on the cell surface only after formation of large molecular complexes with CD3-γ, -δ, -ε, -ζ, and -η chains. If either of the *TCR*-α or β chain genes are not expressed, the TCR*αβ*/CD3 complex cannot be transported to the cellular membrane, and defective complexes accumulate in the cytoplasm *(2,7)*. Thus, inactivating mutations in the *TCRA* or *TCRB* genes among $CD4^+$ T cells can be detected as $CD3^-CD4^+$ mutant cells by two-color flow cytometry using monoclonal antibodies against the CD3 and CD4 molecules. Specifically, the fraction of $CD3^-$ cells in a population of mature $CD4^+$ T cells is considered to be the total Mf for both the *TCRA* and *TCRB* genes in $CD4^+$ T cells. The background Mf of $CD3^-$ cells in populations of human and mouse mature $CD4^+$ T cells increases significantly with age *(2,8)* but is about 2×10^{-4} *(2,3,9–11)*. *TCR* mutants were found to be dose-dependently induced in normal $CD4^+$ T cells and in a lymphoma cell line by in vitro exposure to ionizing radiation *(12–14)* or chemicals *(12)*.

The *TCR* mutation assay can be used to monitor human exposure to environmental mutagens. For example, it has been applied to lymphocytes from cancer patients who had recently received radiotherapy *(9,14,15)* or chemotherapy *(16)*, from patients who had been treated during the 1930s and 1940s with Thorotrast, a colloidal preparation of radioactive thorium-232 used as a radiological contrast medium *(9,17)*, from a person who was heavily exposed to radiation during the 1986 Chernobyl accident *(9)*, from clean-up workers in the Chernobyl accident *(10)*, and from the residents in a radioactively contaminated area near Chelyabinsk in Russia *(18)*. Although statistically significant dose-dependent increases in *TCR* Mf were found in these individuals, no significant elevation was detected in atomic bomb survivors who were exposed to radiation many years ago *(9)*. This is consistent with the observation that elevated Mfs in radiotherapy patients decline gradually to background levels within about 10 yr after exposure (half-life: about 2 yr) *(15,19)*. Although expression of a *TCR* mutant phenotype can require as long as several months in vivo, we have improved the assay to shorten the expression time of the *TCR* mutant phenotype by using growth stimulation of lymphocytes in culture *(14)*. The Mf of *TCR* was found to be elevated in patients with autosomal recessive inherited diseases with defective DNA repair and premature aging, such as ataxia telangiectasia *(2,11)*, Fanconi's anemia *(2)*, Werner's syndrome *(20)*, and Bloom's syndrome *(20,21)*.

We have used a mouse model to demonstrate the in vivo kinetics and dose response of radiation-induced *TCR* mutations *(3)*. In this system, expression of the *TCR* mutant phenotype reached a peak about 2 wk after whole-body irradiation. The Mf then decreased, with a half-life of about 2 wk. We have also reported on the influence of the genetic background on both spontaneous and radiation-induced mutagenesis *(3)*. Using mutant mice, including bioengineered transgenic knockout mice, we have analyzed the role of the *p53* gene in *TCR* mutagenesis *(22)*.

Both human peripheral blood mononuclear cells and mouse T-cell-enriched splenocytes have been used as the target cells for the *TCR* mutation assay. This chapter gives precise methods for the preparation of these target cells and for the flow cytometric procedures used to detect and quantify $CD3^-$ cell fractions among $CD4^+$ T-cell populations.

2. Materials

2.1. Preparation of Human Peripheral Blood Mononuclear Cells

1. Heparinized peripheral blood (3–5 mL).
2. Ficoll-Hypaque solution (specific density 1.077; e.g., Lymphocyte Separation Medium ICN Biomedicals, Aurora, OH).
3. 15-mL polypropylene centrifuge tube.
4. Phosphate-buffered saline (PBS; e.g., Sigma, St. Louis, MO).
5. PBS containing 2.5% fetal calf serum (FCS; Gibco-BRL, Grand Island, NY); heat-inactivated for 30 min at 56°C; PBS-S.
6. Hemacytometer (e.g., Becton Dickinson Primary Care Diagnostics, Sparks, MD).
7. Turk's solution (e.g., Merck, Darmstadt, Germany).
8. 0.4% Trypan blue stain (e.g., Gibco-BRL).

2.2. Preparation of T-Cell-Enriched Mouse Splenocytes

1. 60 × 15-mm Plastic Petri dish (e.g., Becton Dickinson Labware, Franklin Lakes, NJ).
2. Iris scissors and forceps.
3. Frosted glass slides.
4. RPMI-1640 (e.g., Sigma) containing 10% heat-inactivated FCS, 2 m*M* L-glutamine, 100 U/mL penicillin, and 100 μg/mL streptomycin (complete RPMI).
5. 15-mL Polypropylene centrifuge tube.
6. 200-μm Mesh nylon screen.
7. Hemacytometer.
8. 0.4% Trypan blue stain.
9. Nylon wool (e.g., Polysciences, Warrington, PA).
10. 5-mL Disposable syringe.
11. Three-way disposable stopcock.
12. 19- and 23-gage Needles.
13. Cell culture incubator.
14. Parafilm (or Saran Wrap).

2.3. Immunofluorescence Staining

1. Fluorescein isothiocyanate (FITC)-labeled antihuman CD4 monoclonal antibody (Leu-3 antibody, BD Biosciences, San Jose, CA).
2. Phycoerythrin (PE)-labeled antihuman CD3ε monoclonal antibody (Leu-4 antibody, BD Biosciences).
3. FITC-labeled antimouse CD4 monoclonal antibody (CT-CD3 antibody, Caltag Laboratories, Burlingame, CA).
4. PE-labeled antimouse CD3ε monoclonal antibody (145-2C11 antibody, BD Pharmingen Biosciences, San Diego, CA).
5. PBS containing 0.01% NaN_3 and 1% FCS (PBS-NS).
6. PBS-NS containing 10 μg/mL propidium iodide.
7. 1.5-mL Eppendorf tube.
8. 5-mL Polystyrene round-bottomed tube (Becton Dickinson Labware).

2.4. Flow Cytometry

1. Flow cytometer (e.g., FACScan, BD Biosciences) installed with computer software for data acquisition and analysis (e.g., CELLQuest, BD Biosciences).

3. Methods

3.1. Preparation of Human Peripheral Blood Mononuclear Cells (see Note 1)

1. Place heparinized blood (3–5 mL) into a 15-mL centrifuge tube.
2. Add an equal volume of PBS at room temperature and mix well.
3. Slowly layer the Ficoll-Hypaque solution underneath the blood/PBS mixture by placing the tip of the pipet containing the Ficoll-Hypaque at the bottom of the sample tube. Use 3 mL Ficoll-Hypaque per 10 mL blood/PBS mixture.
4. Centrifuge for a total of 30 min at 400*g* at room temperature with no brake. (Slowly raise the centrifuge speed to 400*g*.)
5. Using a pipet, remove the upper layer containing the plasma and platelets. Using another pipet, transfer the mononuclear cell layer (interface between the upper and Ficoll-Hypaque layers) to a new 15-mL centrifuge tube.
6. Wash cells by adding excess PBS-S (about three times the volume of the mononuclear cell layer) at room temperature and centrifuging for 10 min at 510*g*.
7. Discard supernatant, resuspend cells in 10 mL PBS-S, and centrifuge for 10 min at 240*g*.
8. Repeat **step 7**.
9. Discard supernatant and resuspend cells in 1 mL PBS-S.
10. Count mononuclear cells in Turk's solution using a hemacytometer and calculate cell yield. Use trypan blue exclusion to determine cell viability. Average yield is about 1×10^6 viable mononuclear cells from 1 mL blood.

3.2. Preparation of T-Cell-Enriched Mouse Splenocytes

1. Sacrifice mice in a humane manner. Make a 1.5-cm incision at the left of the peritoneal wall with scissors. Gently pull the spleen free of the peritoneum, tearing the connective tissue behind the spleen.
2. Place the spleen in a 60 × 15-mm plastic Petri dish containing 3 mL complete RPMI. With scissors, cut the spleen into several pieces.
3. By rubbing between the frosted faces of two glass slides, mash the spleen pieces until mostly fibrous tissue remains.
4. Expel cell suspension into a 15-mL plastic centrifuge tube through a 200-μm-mesh nylon screen. Wash Petri dish with about 4 mL complete RPMI.
5. Centrifuge cell suspension at 240*g* for 10 min. Resuspend cell pellet in 10 mL complete RPMI and count cells with trypan blue exclusion using a hemacytometer for determining cell yield and viability. The viable cell yield per normal spleen is $5–20 \times 10^7$, depending on the mouse strain and age.
6. Centrifuge again and resuspend in 0.5 mL complete RPMI.
7. Prepare a nylon wool column by packing 0.3 g nylon wool in a 5-mL disposable syringe (*see* **Note 2**). Insert the plunger, and press firmly to compact the nylon wool.
8. Clamp the sterilized nylon wool column to a ring stand. Attach both to a three-way stopcock in an open position and a 19-gage needle.
9. Equilibrate the column by running 10 mL of 37°C warmed complete RPMI through the column. Remove trapped air bubbles by firmly tapping on the sides of the column until no dry areas are visible. Finally, tamp down the nylon wool with a pipet to compact the nylon and extrude any additional trapped air.
10. Close the stopcock and cover the nylon wool with 1–2 mL warmed complete RPMI to prevent drying. Incubate the column in an upright position for 45 min at 37°C, 5% CO_2 in a humidified incubator.
11. Warm cell suspension at 37°C.

12. Open the stopcock and allow the medium to drain completely. Using a Pasteur pipet, add dropwise 0.5 mL warmed cell suspension onto the nylon wool and again allow to drain completely. Close the stopcock, and cover the top of the column with plastic (Parafilm or Saran Wrap).
13. Incubate the column for 1 h in an upright position in a 37°C, 5% CO_2 humidified incubator.
14. Remove the column from the incubator, and clamp to the ring stand. Replace the 19-gage needle with a 23-gage needle.
15. Open the stopcock and elute the column with 10 mL total warmed complete RPMI. Collect the effluent (nonadherent) cells in a 15-mL centrifuge tube.
16. Centrifuge harvested cells at 240*g*, 4°C for 10 min.
17. Discard supernatant and resuspend cells in 10 mL complete RPMI.
18. Count cells with trypan blue exclusion using a hemacytometer for determining cell yield and viability. Average yield is about 2–3 $\times 10^7$ T-cell–enriched cells from a spleen (*see* **Notes 3** and **4**).

3.3. Immunofluorescence Staining

1. Transfer 2 $\times 10^6$ human peripheral blood mononuclear cells or mouse T-cell-enriched splenocytes suspended in PBS-NS to a 1.5-mL Eppendorf tube, and centrifuge at 340*g*, 4°C for 2 min.
2. Discard supernatant, and add 2 μg each of FITC-labeled antihuman or -mouse CD4 and PE-labeled antihuman or -mouse CD3 antibodies to the cell pellet, mix well, and incubate for 30 min on ice.
3. Wash cells by adding 0.75 mL PBS-NS and centrifuging at 340*g*, 4°C for 2 min.
4. Discard supernatant and resuspend cells in 0.5 mL PBS-NS containing propidium iodide to stain dead cells. Transfer cell suspension to a 5-mL polystyrene tube for flow cytometry.

3.4. Flow Cytometry (see Note 5)

1. *TCR* mutant $CD4^+$ T cells ($CD3^-/CD4^+$) can be measured using a FACScan installed with the operation and analysis software CELLQuest. Set up the FACScan and CELLQuest, and optimize settings according to the manufacturer's instructions (*see* **Note 6**).
2. First, run a small number of the stained lymphocytes (about 1000 events) through the FACScan. Set a gate for the lymphocyte fraction using the forward and side light scatter (FSC and SSC) profile (**Fig. 1A** and **B**).
3. Acquire and store FL1 (CD4 FITC fluorescence) and FL2 (CD3 PE fluorescence) data for a minimum of 500,000 lymphocyte-gated events (*see* **Note 7**).
4. Display acquired data on the screen in histograms of FL1 (CD4) and FL2 (CD3) and in density plots of FL1 vs. FL2 (**Fig. 1B**, **C**, **E**, and **F**). Obtain the peak fluorescence intensities (channel number) of the FL1 (CD4) and FL2 (CD3) of normal $CD3^+/CD4^+$ cell population in the histograms by gating this population in the density plot. (Gate out propidium iodide-stained dead cells from the population; **Fig. 1B**, **C**, **E**, and **F**).
5. Set a mutant window on the region for $CD3^-/CD4^+$ in the density plot as follows. Set the left and right limits of FL1 at the half and two times values of the peak intensity of FL1 (CD4) for normal $CD3^+/CD4^+$ cells, respectively. Set the upper limit of the FL2 for the mutant window at the 1/25 value of the peak intensity of CD3 for normal $CD3^+/CD4^+$ cells as mentioned above, and set the lower limit at 10^0 (*see* **Note 8**).
6. Calculate the Mf as the number of events in the mutant window (**Fig. 1B**, **C**, **E**, and **F**) divided by the total number of events corresponding to $CD4^+$ cells.

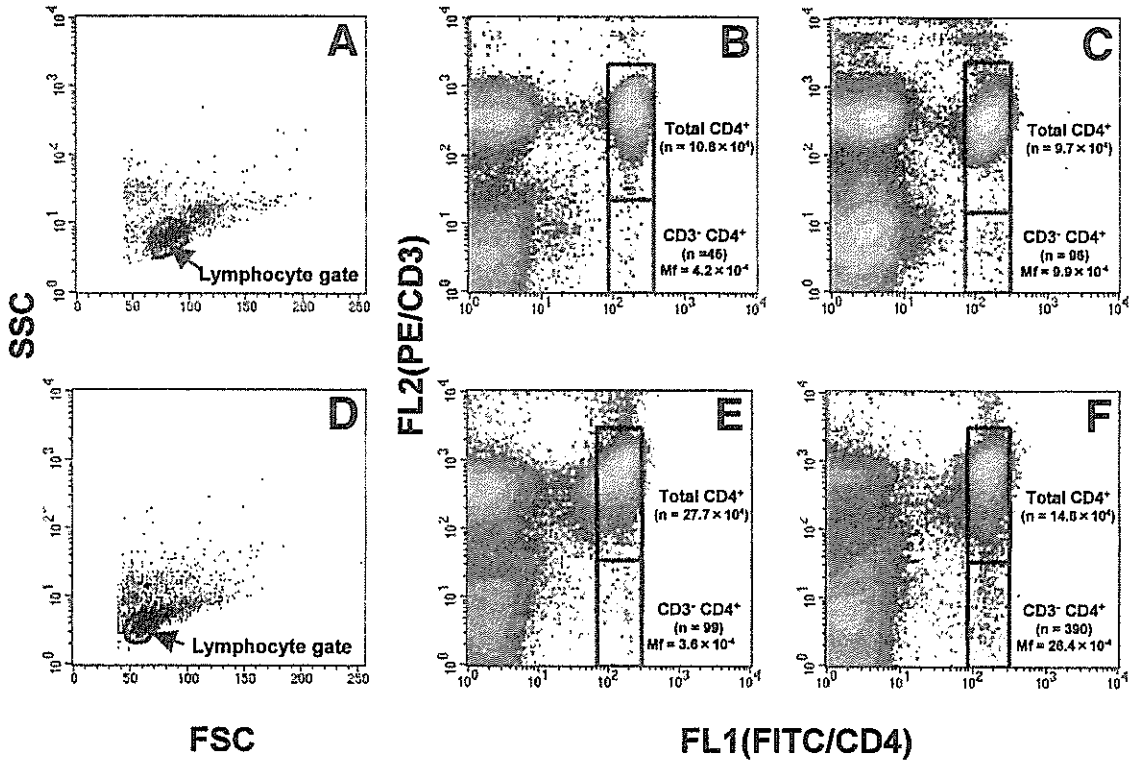

Fig. 1. Representative flow cytograms of human peripheral blood mononuclear cells (**A–C**) and nylon-wool-passed mouse splenocytes (**D–F**) stained with FITC-labeled anti-CD4 (FL1) and PE-labeled anti-CD3 (FL2) monoclonal antibodies. (**A** and **D**) Gates for lymphocytes on forward and side light scatter (FSC and SSC) profiles (dot plot). (**B**, **C**, **E**, and **F**) Windows for total $CD4^+$ and mutant $CD3^-/CD4^+$ T cells on fluorescence profiles (density plot). The number of events in each window is shown in each panel. The mutant fraction (Mf) was calculated as the number of events in the mutant window divided by the number of events in the total $CD4^+$ T cells. Events representing the highest FL2 fluorescence (nearly 10^4) are dead cells stained with propidium iodide. (**A** and **B**) Laboratory control (48-yr-old male). (**C**) A patient who had received Thorotrast. (**D** and **E**) C57BL/6 mouse (4-mo-old female). (**F**) C57BL/6 mouse irradiated with 2.5 Gy X-rays (2 wk after whole-body irradiation).

4. Notes

1. Tubes for one-step mononuclear cell separation from whole blood are commercially available (e.g., BD Vacutainer CPT tube, Becton Dickinson Primary Care Diagnostics). These tubes contain anticoagulant (sodium heparin or sodium citrate) and the cell separation medium, which is composed of a polyester gel and a density gradient liquid.
2. Prepacked nylon wool fiber columns are also commercially available (e.g., Polysciences).
3. Generally, effluent cells are 80–90% T cells and 10–20% B cells and macrophages. Viable cell yield after nylon column passage is generally 15–20% of the initial number of cells loaded on the column.
4. T-cell-enriched mouse splenocytes can also be prepared using a magnetic cell sorting system (MACS) for the *TCR* mutation assay. A pan-T-cell isolation kit containing cock-

tail of magnetic beads for depleting non-T cells is commercially available (e.g., Miltenyi Biotec, Bergish-Gladbach, Germany).

5. The general principles of methodological flow cytometry have been described elsewhere *(23)*.
6. Setup procedures for flow cytometry using the FACScan are described elsewhere *(24)*.
7. Data correlated by four parameters (FSC, SSC, FL1, and FL2) can be acquired and stored if disk storage space is large enough. The lymphocyte gate should be set on the light scatter profile for the mutant analyses of the stored four-parameter data.
8. The mutant window may be set by other reasonable rules. For example, the upper limit of the mutant window can be set at the value of the mean plus 3 standard deviations of PE fluorescence intensity (FL2) of $CD3^-/CD4^-$ cells *(10)*.

Acknowledgments

The authors would like to acknowledge M. Yamaoka and K. Koyama for excellent technical help and C. A. Waldren for valuable suggestions.

References

1. Cole, J. and Skopek, T. R. (1994) Somatic mutant frequency, mutation rates and mutational spectra in the human population in vivo. *Mutat. Res.* **304,** 33–105.
2. Kyoizumi, S., Akiyama, M., Hirai, Y., Kusunoki, Y., Tanabe, K., and Umeki, S. (1990) Spontaneous loss and alteration of antigen receptor expression in mature CD4+ T cells. *J. Exp. Med.* **171,** 1981–1999.
3. Umeki, S., Suzuki, T., Kusunoki, Y., Seyama, T., Fujita, S., and Kyoizumi, S. (1997) Development of a mouse model for studying in vivo T-cell receptor mutations. *Mutat. Res.* **393,** 37–46.
4. Davodeau, F., Peyrat, M. A., Romagne, F., et al. (1995) Dual T cell receptor beta chain expression on human T lymphocytes. *J. Exp. Med.* **181,** 1391–1398.
5. Padovan, E., Casorati, G., Dellabona, P., Meyer, S., Brockhaus, M., and Lanzavecchia, A. (1993) Expression of two T cell receptor alpha chains: dual receptor T cells. *Science* **262,** 422–424.
6. Malissen, M., Trucy, J., Jouvin-Marche, E., Cazenave, P. A., Scollay, R., and Malissen, B. (1992) Regulation of TCR alpha and beta gene allelic exclusion during T-cell development. *Immunol. Today* **13,** 315–322.
7. Clevers, H., Alarcon, B., Wileman, T., and Terhorst, C. (1988) The T cell receptor/CD3 complex: a dynamic protein ensemble. *Annu. Rev. Immunol.* **6,** 629–662.
8. Akiyama, M., Kyoizumi, S., Hirai, Y., Kusunoki, Y., Iwamoto, K. S., and Nakamura, N. (1995). Mutation frequency in human blood cells increases with age. *Mutat. Res.* **338,** 141–149.
9. Kyoizumi, S., Umeki, S., Akiyama, M., et al. (1992) Frequency of mutant T lymphocytes defective in the expression of the T-cell antigen receptor gene among radiation-exposed people. *Mutat. Res.* **265,** 173–180.
10. Saenko, A. S., Zamulaeva, I. A., Smirnova, S. G., et al. (1998) Determination of somatic mutant frequencies at glycophorin A and T-cell receptor loci for biodosimetry of prolonged irradiation. *Int. J. Radiat. Biol.* **73,** 613–618.
11. Lantelme, E., Mantovani, S., Palermo, B., et al. (2000) Increased frequency of RAG-expressing, CD4(+)CD3(low) peripheral T lymphocytes in patients with defective responses to DNA damage. *Eur. J. Immunol.* **30,** 1520–1525.

12. Mei, N., Kunugita, N., Nomoto, S., and Norimura, T. (1996) Comparison of the frequency of T-cell receptor mutants and thioguanine resistance induced by X-rays and ethylnitrosourea in cultured human blood T-lymphocytes. *Mutat. Res.* **357,** 191–197.
13. Iwamoto, K. S., Mizuno, T., Ito, T., Tsuyama, N., Kyoizumi, S., and Seyama, T. (1996) Gain-of-function *p53* mutations enhance alteration of the T-cell receptor following X-irradiation, independently of the cell cycle and cell survival. *Cancer Res.* **56,** 3862–3865.
14. Ishioka, N., Umeki, S., Hirai, Y., et al. (1997) Stimulated rapid expression in vitro for early detection of in vivo T-cell receptor mutations induced by radiation exposure. *Mutat. Res.* **390,** 269–282.
15. Iwamoto, K. S., Hirai, Y., Umeki, S., et al. (1994) A positive correlation between T-cell-receptor mutant frequencies and dicentric chromosome frequencies in lymphocytes from radiotherapy patients. *J. Radiat. Res.* **35,** 92–103.
16. Hirota, H., Kubota, M., Adachi, S., et al. (1994) Somatic mutations at T-cell antigen receptor and glycophorin A loci in pediatric leukemia patients following chemotherapy: comparison with HPRT locus mutation. *Mutat. Res.* **315,** 95–103.
17. Umeki, S., Kyoizumi, S., Kusunoki, Y., et al. (1991) Flow cytometric measurements of somatic cell mutations in Thorotrast patients. *Jpn. J. Cancer Res.* **82,** 1349–1353.
18. Akleyev, A. V., Kossenko, M. M., Silkina, L. A., et al. (1995). Health effects of radiation incidents in the southern Urals. *Stem Cells* **13(suppl. 1),** 58–68.
19. Umeki, S., Kusunoki, Y., Cologne, J. B., et al. (1998). Lifespan of human memory T-cells in the absence of T-cell receptor expression. *Immunol. Lett.* **62,** 99–104.
20. Kyoizumi, S., Kusunoki, Y., Seyama, T., Hatamochi, A., and Goto, M. (1998) In vivo somatic mutations in Werner's syndrome. *Hum. Genet.* **103,** 405–410.
21. Kusunoki, Y., Hayashi, T., Hirai, Y., et al. (1994) Increased rate of spontaneous mitotic recombination in T lymphocytes from a Bloom's syndrome patient using a flow-cytometric assay at HLA-A locus. *Jpn. J. Cancer Res.* **85,** 610–618.
22. Suzuki, T., Kusunoki, Y., Tsuyama, N., Ohnishi, H., Seyama, T., and Kyoizumi, S. (2001) Elevated in vivo frequencies of mutant T cells with altered functional expression of the T-cell receptor or hypoxanthine phosphoribosyltransferase genes in *p53*-deficient mice. *Mutat. Res.* **483,** 13–17.
23. Shallow, S. O. (1999) Overview of flow cytometry, in *Current Protocols in Immunology* (Coligan, J. E., Kruisbreek, A. M., Margulies, D. H., Shevach, E. M., and Strober, W., eds.), John Wiley & Sons, New York, Units 5.1 and 5.2.
24. Otten, G., Yokoyama, W. M., and Holmes, K. L. (1999) Flow cytometry analysis using the Becton Dickinson FACScan, in *Current Protocols in Immunology* (Coligan, J. E., Kruisbreek, A. M., Margulies, D. H., Shevach, E. M., and Stroer, W., eds.), John Wiley & Sons, New York, Unit 5.4.

RADIATION RESEARCH 161, 642–647 (2004)
0033-7587/04 $15.00

An Association between Oxidative Stress and Radiation-Induced Lymphomagenesis

Gen Suzuki,[a,1] Yoshiya Shimada,[c] Tomonori Hayashi,[b] Makoto Akashi,[d] Toshiyasu Hirama[d] and Yoichiro Kusunoki[b]

[a] *Department of Clinical Studies and* [b] *Department of Radiobiology/Molecular Epidemiology, Radiation Effects Research Foundation, 5-2 Hijiyama Park, Hiroshima 732-0815, Japan; and* [c] *Research Center for Radiation Safety and* [d] *Research Center for Radiation Emergency Medicine, National Institute of Radiological Sciences, 4-9-1, Anagawa, Inage-ku, Chiba 263-8555, Japan*

Suzuki, G., Shimada, Y., Hayashi, T., Akashi, M., Hirama, T. and Kusunoki, Y. An Association between Oxidative Stress and Radiation-Induced Lymphomagenesis. *Radiat. Res.* 161, 642–647 (2004).

It is generally thought that reactive oxygen species (ROS) play an important role in carcinogenesis. However, direct evidence supporting this idea is still lacking. In the present study, we measured ROS in thymocytes at the thymic prelymphoma stage in C57BL/6 mice. Mice ($n = 20$) were irradiated at 1.6 Gy/week for 4 consecutive weeks and the levels of ROS were measured 8 to 11 weeks later by dehydrorhodamine 123, which accumulated in mitochondria and became fluorescent dye upon oxidation. Unirradiated littermates ($n = 17$) served as controls. Thymic prelymphoma cells were diagnosed by the aberrant CD4/CD8 staining profile and monoclonal or oligoclonal T-cell receptor gene rearrangement. A significant fraction of mice (11/13) bearing thymic prelymphoma cells exhibited elevated levels of ROS in thymocytes ($P < 0.001$). The result is consistent with the hypothesis that ROS may play an important role in radiation carcinogenesis. © 2004 by Radiation Research Society

INTRODUCTION

There is increasing evidence that most cancers contain multiple mutations, and the accumulation of dysfunction in several key molecules seems essential for carcinogenesis (*1*). In normal cells, the mutation rate is low, of the order of 10^{-10} mutations per nucleotide per cell per generation, which is insufficient to account for the large numbers of mutations observed in cancer cells (*2*). It is believed that only cells with mutator phenotypes or genomic instability will accumulate genetic alterations required for carcinogenesis. Radiation is a well-known mutagen that induces many kinds of neoplasms (*3*). Radiation can acutely induce DNA double-strand breaks, single-strand breaks, and crosslinking between DNA and protein in a dose-dependent manner (*4*). The impact of these alterations on cells may either initiate the process of multistage carcinogenesis in stem cells or accelerate the process already initiated in cells by other mutagens. Furthermore, radiation is believed to have a long-lasting effect on the progeny of irradiated cells by inducing genomic instability, and it may shorten the period required for the progression of each step in multistage carcinogenesis (*5–7*). However, the molecular mechanisms of induction of genomic instability by radiation have not been fully elucidated.

Reactive oxygen species (ROS) are generated constantly in cells and injure DNA in the nucleus as well as deoxynucleotide triphosphate in its cellular pool. Y-family polymerases erroneously incorporate an oxidized deoxynucleotide into DNA or repair an oxidized DNA erroneously (*8, 9*). Thus an increase in the production of ROS may cause genomic instability and facilitate the process of multistage carcinogenesis. In support of this idea, mice with a mutation in the cytochrome b subunit exhibited an increase in ROS production and a high mutation rate.[2] Recently, it became evident that radiation elevates ROS in the progeny of irradiated cells *in vitro* (*10–12*), which forced us to test the hypothesis that one of the mechanisms of radiation-induced genomic instability might be the prolonged elevation of ROS *in vivo*. To test this, we took advantage of a radiation-induced thymic lymphoma model in which more than 90% of irradiated B10 mice generated thymic lymphoma (*13*), and thymic prelymphoma cells could be detected by the presence of oligoclones having a particular T-cell receptor (TCR) gene rearrangement in the thymus. ROS were measured directly in mitochondria by the oxidation-sensitive fluorescent probe dihydrorhodamine 123 (DHR) (*10*). Our results clearly demonstrated significant associations of elevated oxidative stress with aberrant CD4/CD8 staining profile and mono- or oligoclonal TCR gene rearrangement in thymocytes at the thymic prelymphoma stage in irradiated mice. This information supported the hypothesis that an increase in generation of ROS might be one of the mech-

[1] Address for correspondence: Department of Clinical Studies, Radiation Effects Research Foundation, 5-2 Hijiyama Park, Minami-ku, Hiroshima 732-0815, Japan; e-mail: gsuzuki@rerf.or.jp.

[2] N. Ishii, Tokai University School of Medicine, Kanagawa, Japan, personal communication.

anisms of radiation-induced genomic instability that could lead to lymphomagenesis.

MATERIALS AND METHODS

Mice

C57BL/6 mice were bred and kept in our conventional animal facility in the National Institute of Radiological Sciences, Chiba. Four-week-old female mice were X-irradiated with 1.6 Gy four times for 4 consecutive weeks using a Pantak X irradiator (Pantak Ltd., East Haven, CT) at 200 kVp, 20 mA with 0.5 mm copper and aluminum filters. Unirradiated female littermates served as controls. Several weeks after irradiation, mice were transferred to the Radiation Effects Research Foundation, Hiroshima, and kept in a conventional animal facility. Three to five irradiated mice and unirradiated littermates were killed humanely 8 to 11 weeks after the last irradiation, as indicated. The chairman of the institutional animal use committee reviewed and assured that all experiments had been done following the International Guiding Principles for Biomedical Research Involving Animals issued by WHO in 1985.

Flow Cytometry Analyses

Thymocytes (1×10^6) were suspended in 1 ml of RPMI-1640 medium supplemented with 2% fetal bovine serum. Cells were stored in the dark and incubated with DHR (Molecular Probes, Eugene, OR) at a final concentration of 1 μM at 37°C for 80 min. DHR is a pro-fluorescent dye that accumulates in mitochondria and becomes fluorescent rhodamine-123 upon oxidation by ROS. After washing once with medium, cells were analyzed by flow cytometry (FACScan Becton Dickinson, Mountain View, CA). The mean fluorescence intensity was calculated using CellQuest software (Becton Dickinson). Thymocytes were stained with PE-conjugated anti-CD4 and FITC-conjugated anti-CD8 and analyzed with the FACScan. In the case of three-color staining, cells incubated with DHR were further reacted with CyChrome-conjugated anti-CD4 and PE-conjugated anti-CD8. All fluorochrome-labeled reagents were purchased from PharMingen (San Diego, CA).

TCR Gene Rearrangement

Genomic DNA was extracted from thymocytes using Qiagen Genomic-tip 100 (Qiagen, Tokyo). Specific primers and PCR conditions for the amplification of the genomic DNA segment containing TCR Dβ and Jβ genes were reported elsewhere (*14*). By combining Dβ sense primer and Jβ anti-sense primer, i.e. Dβ1-Jβ1.5, Dβ1-Jβ1.6, Dβ1-Jβ2.6 and Dβ2-Jβ2.6, every TCR Dβ-Jβ rearrangement band could be detected (*14*).

Statistical Analyses

Fisher's exact probability test was used.

RESULTS AND DISCUSSION

More than 90% of the irradiated mice developed thymic lymphoma after an average latent period of 200 days in B10 mice (*13*). Since some mice developed thymic lymphoma as early as 8 weeks, we performed flow cytometry analyses 8 to 11 weeks after irradiation. As shown in Table 1, only 2 of 20 irradiated mice bore overt thymic lymphoma, and 7 showed a decreased number of thymocytes (Table 1). Normal thymocytes are composed of four subpopulations, $CD4^-CD8^-$ double negative (DN), $CD4^+CD8^+$ double positive (DP), $CD4^+CD8^-$ single positive (SP), and $CD4^-CD8^+$ SP cells. DN cells are the most immature cells that differentiate into DP cells through intermediate CD8 SP cells. Only a small fraction of DP cells differentiate into either CD4 or CD8 SP cells after so-called thymic selection, and these SP cells immigrate to peripheral lymphoid organs (*15, 16*). Figure 1A shows the representative staining profiles of these four thymocyte subpopulations in normal thymus. In contrast to control mice, 13 of 17 irradiated mice showed aberrant staining profiles (Table 1), in which CD8 SP and/or DP cells increased independent of thymocyte cell numbers (Fig. 1B–D).

TABLE 1
Effect of Radiation on the Regeneration of Thymocytes

Weeks after irradiation	Cell count[a] ($\times 10^8$)	CD4/CD8 staining profile	Elevation in ROS[b]
8	4.2*[c]	Not done	no
8	0.5*	Not done	yes (1.7)
8	1.2	Not done	no
9	0.6*	normal	yes (1.7)
9	1.9	normal	yes (1.5)
9	6*[c]	DP/CD8	no
9	0.14*	CD8	yes (2.5)
9	2.5*	DP/CD8	no
9	0.16*	DP/CD8	yes (3.3)
9	1.7	DP/CD8	yes (1.5)
10	1.3	normal	no
10	1.2	DP	yes (1.3)
10	0.58*	DP/CD8	yes (1.9)
10	2.4	CD8	yes (1.7)
10	2.3	CD8	yes (2.1)
11 (no. 6)[d]	2.3	CDP/CD8	yes (1.5)
11 (no. 7)[d]	1.7	normal	no
11 (no. 8)[d]	0.53*	DP/CD8	yes (2.2)
11 (no. 9)[d]	1.8	DP	yes (1.4)
11 (no. 10)[d]	0.55*	DP	yes (1.6)

[a] Seventeen littermates served as controls. Thymocyte counts in control mice were $1.65 \pm 0.43 \times 10^8$ ($n = 17$). *Those cell counts were more or less than 2 SD away from the thymocyte counts in the control mice.

[b] Elevation of ROS was determined if the mean fluorescence intensity of DHR staining exceeded more than 3 SD of the control mice. The elevation in ROS was measured as the ratio between the mean fluorescence intensity of each experimental mouse and the average mean fluorescence intensity of the control mice.

[c] These two mice were diagnosed as having thymic lymphoma.

[d] These five mice were tested for TCRβ gene rearrangement. Numbers in parentheses are numbers of the mice in the experiment in Fig. 2.

Next we measured the levels of ROS in mitochondria in thymocytes by DHR staining. In each experiment, the reference level of ROS in mitochondria was determined in three to five control mice, and the mean fluorescence intensity of DHR staining was calculated. We judged a mouse to have elevated levels of ROS if the mean fluorescence intensity of DHR staining was more than the mean plus 3 SD of control mice. The levels of ROS in normal mice were fairly constant from mouse to mouse (Fig. 1E). In contrast, 14 of 20 irradiated mice showed an increase in ROS in mitochondria (Table 1). Representative DHR staining profiles are shown in the lower panel of Fig. 1. The difference in DHR staining levels was not due solely to the difference

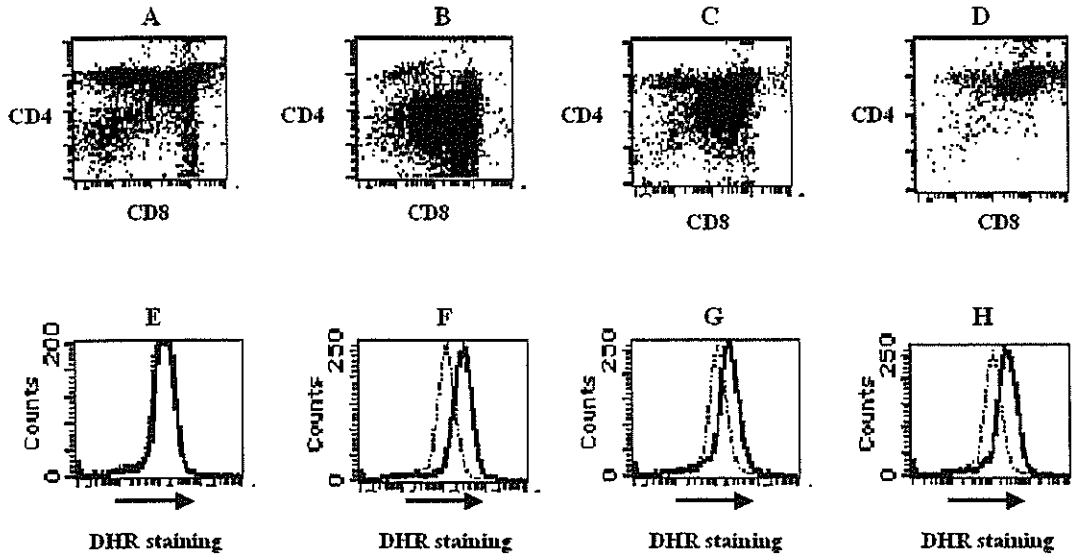

FIG. 1. Irradiated thymus bears an aberrant T-cell subpopulation with elevated ROS in mitochondria. Representative double-staining profiles of CD4 and CD8 are shown. Panel A: normal mouse; panel B: aberrant increase in $CD8^+$ cells; panel C: aberrant increase in $CD8^+$/DP cells; panel D: aberrant increase in DP cells; panel E: the overlay histograms of DHR staining profile in five control mice; panels F, G, H: DHR staining profile of an irradiated mouse (solid line) overlaid with that of a control mouse (dotted line). Thymocytes in panels B and panels F, C and G, and panels D and H were from the same individual mice.

in cell size between irradiated and normal mice; when the same cell-sized thymocytes as determined by forward scatter size in the flow cytometry analysis were compared, the levels of DHR staining were brighter in thymocytes from irradiated mice than in those from control mice.

The association between the CD4/CD8 staining profile and ROS levels was analyzed in 17 irradiated and 17 control mice. Eleven of 13 mice with an aberrant CD4/CD8 staining profile exhibited increased levels of ROS while only 2 of 21 mice with normal CD4/CD8 staining did (Table 2). Thus an aberrant CD4/CD8 staining status was significantly associated with an increase in ROS in mitochondria ($P < 0.001$).

Next we assessed whether elevated levels of ROS were associated with the clonal expansion of thymic prelymphoma cells that showed an aberrant CD4/CD8 staining profile in five control and five irradiated mice by PCR. Mature T cells bear heterodimeric receptors: either TCRαβ or TCRγδ. In the thymus, T cells sequentially rearrange the TCR-Vβ, -Dβ, and -Jβ genes at the DN stage and the TCRα gene at the DP stage. Using four combinations of Dβ-sense and Jβ anti-sense primers, all possible combinations of TCR Dβ-Jβ gene rearrangements were detected as different PCR bands of almost the same intensity in normal thymocytes (Fig. 2, mouse nos. 1–5). In contrast, four of five irradiated mice showed monoclonal or oligoclonal bands; Dβ1-Jβ2.4 band in no. 6, Dβ1-Jβ2.5 band in no. 8, Dβ1-Jβ1.5, Dβ2-Jβ2.2, Dβ1-Jβ2.5 and germ-line bands in no. 9, Dβ1-Jβ1.4, Dβ2-Jβ2.2, Dβ2-Jβ2.3 and germ-line bands in no. 10 (Fig. 2A–D). As indicated in Table 1, these four mice showed aberrant CD4/CD8 profiles and elevated ROS, while mouse no. 7 showed a normal CD4/CD8 staining profile and reference levels of ROS. There was a significant association between elevated ROS and mono- or oligoclonal TCRβ gene rearrangement (Table 3). Collectively, these data indicated that monoclonal or oligoclonal expansion of thymic prelymphoma cells was associated with aberrant CD4/CD8 staining and an increase in ROS in mitochondria.

Radiation acutely generates both short-lived and long-

TABLE 2
Association between Elevated ROS and Aberrant CD4/CD8 Staining Profile

	CD4/CD8 staining profile[a]		
	Normal	Aberrant	Total
Normal ROS level	19	2	21
Elevated ROS level	2	11[b]	13
Total	21	13	34

[a] Seventeen irradiated and 17 control mice were examined for CD4/CD8 staining and ROS levels.

[b] Statistically significant by Fisher's exact probability test (P = 0.000018).

→

FIG. 2. Mono- or oligoclonal TCRβ gene rearrangement is detected in thymic prelymphoma cells. Schematic presentation of TCR Dβ and Jβ gene segments and four primer sets used for PCR: panel A: Dβ1-Jβ1.5; panel B: Dβ1-Jβ1.6; panel C: Dβ2-Jβ2.6; panel D: Dβ1-Jβ2.6 (upper row). PCR was performed using genomic DNA of individual thymus from normal (lanes 1 to 5) and irradiated (lanes 6 to 10) mice. The marker lane was the mixture of λDNA digested by *Hin*dIII and φX174 DNA digested by *Hae*III.

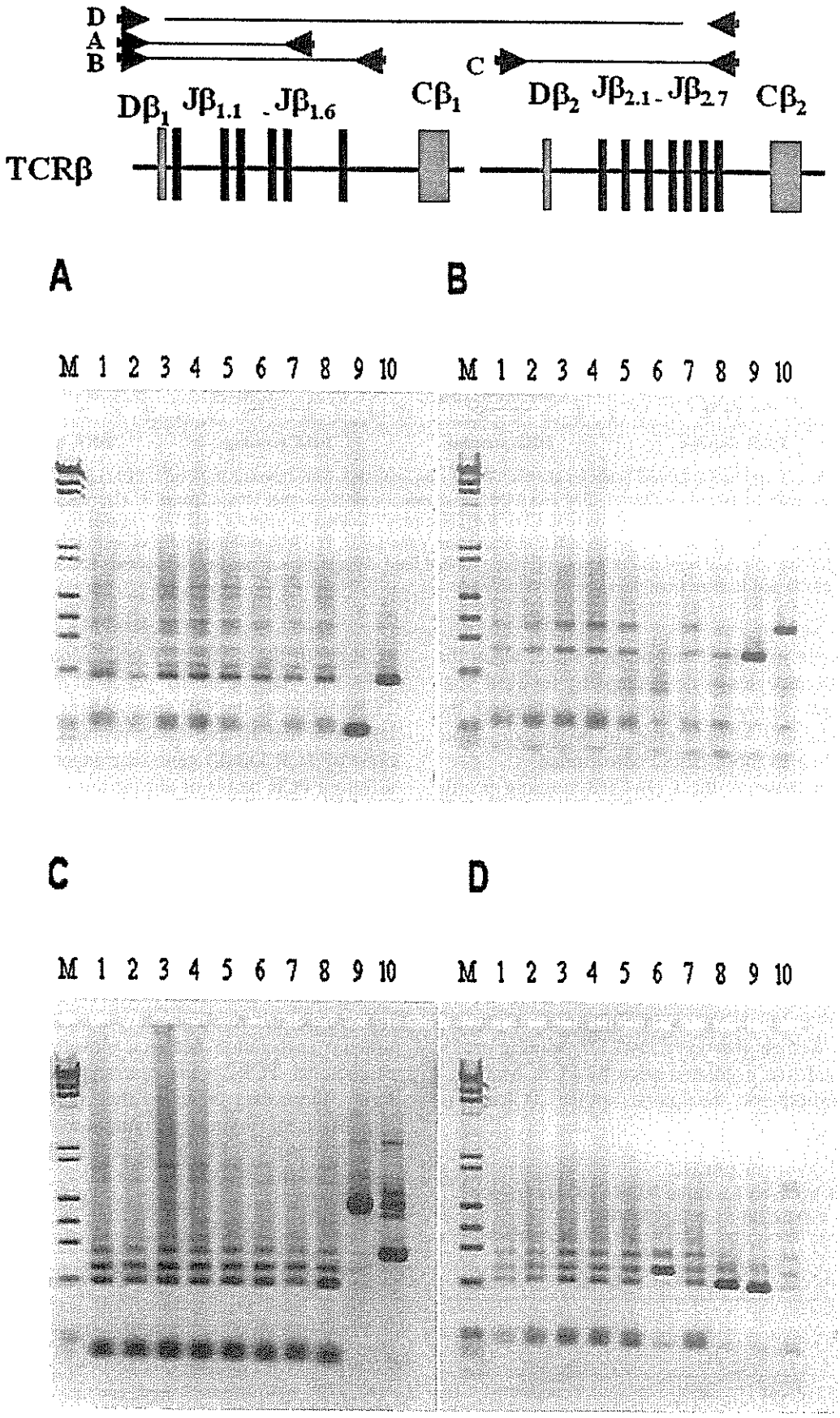
D
A
B
C
Dβ1 Jβ1.1 - Jβ1.6
Cβ1
Dβ2 Jβ2.1 - Jβ2.7
Cβ2
TCRβ
A
B
M 1 2 3 4 5 6 7 8 9 10
M 1 2 3 4 5 6 7 8 9 10
C
D
M 1 2 3 4 5 6 7 8 9 10
M 1 2 3 4 5 6 7 8 9 10

TABLE 3
Association between Elevated ROS Levels and Mono- and Oligoclonal TCRβ Gene Rearrangement

	TCRβ gene rearrangement[a]		
	Polyclonal	Mono- or oligoclonal	Total
Normal ROS	6	0	6
Elevated ROS	0	4[b]	4
Total	6	4	10

[a] Five irradiated and five control mice were examined for TCRβ gene rearrangement. Clonality was judged by a pattern of TCR Dβ-Jβ gene rearrangement shown in Fig. 2.

[b] Statistically significant by Fisher's exact probability test (P = 0.0048).

lived radicals (*17, 18*). Half-lives of radicals are generally short, and even a long-lived sulfinyl radical has a half-life of 20 h (*17*). However, Clutton *et al.* first reported that the progeny of irradiated bone marrow cells in culture exhibited an increase in production of ROS even 7 days after irradiation and proposed a hypothesis that enhanced and persistent oxidative stress might cause genomic instability after irradiation (*10*). Recently, two other groups confirmed the observation of Clutton *et al.* using normal fibroblasts or cell lines (*11, 12*). Since generation of ROS *in vitro* might be influenced by culture conditions such as confluence (*11*), it is important to investigate whether the progeny of irradiated stem cells exhibit an increase in production of ROS *in vivo*. In the present study we provided evidence that the hypothesis of Clutton *et al.* may also be plausible *in vivo*.

It was noted that the elevation of ROS was not completely associated with thymic prelymphomas or lymphomas; two of the irradiated mice with normal CD4/CD8 staining profiles exhibited elevated ROS levels, while three irradiated mice with either lymphoma or an aberrant CD4/CD8 staining profile showed normal levels of ROS. The results imply that ROS may be important but not essential for the whole process of lymphomagenesis. Once the critical stage for lymphomagenesis has passed, ROS may no longer be required, and in some mice, no elevation was observed when mice were killed.

The mechanisms resulting in an increase in ROS in mitochondria in thymic prelymphoma cells were beyond the scope of the present study. The following, however, are plausible mechanisms. First, DNA damage might generate ROS by activating Trp53 (*19, 20*). Limoli reported that chromosomally unstable cells showed elevated levels of ROS (*21*). In the case of immature T cells, DN and DP cells make endogenous DNA double-strand breaks by RAG1/RAG2 recombinase in the process of TCR V(D)J gene rearrangement. The levels of DHR staining were 2.2-fold higher in DN and DP cells than those in CD4 and CD8 SP cells in normal mice (data not shown). However, the levels of DHR staining in thymic prelymphoma cells were higher than those in normal thymocytes, 85% of which were DP cells, indicating that activation of RAG1/RAG2 recombinase was insufficient to elevate ROS to the levels observed in thymic prelymphoma cells. Second, the increase in production of ROS might be caused by mutations of genomic genes that affect the function of either mitochondrial respiratory chains or cellular redox proteins (*22, 23*). Third, radiation might affect mitochondrial DNA, which plays a role in the respiratory chain (*22*). Although there are hundreds to thousands of mitochondria in one cell, mitochondria affected by mutagens can be distributed unevenly into daughter cells and can accumulate sufficiently to elevate ROS levels in the progeny (*22, 24*). It was also reported that the accumulation of mitochondria lacking respiratory function disrupted the pro-oxidant/antioxidant balance in cells and thereby elevated levels of ROS (*25*). Fourth, radiation might have affected stromal cells in the thymus so as to produce excess amounts of bioactive substances such as chemokines or proinflammatory cytokines capable of up-regulating ROS levels in thymocytes. Further studies are needed to investigate the mechanisms of elevated ROS levels in thymic prelymphoma cells.

Finally, the present study clearly demonstrated an association between ROS and lymphomagenesis, suggesting that mitochondria play an important role in multistage carcinogenesis.

ACKNOWLEDGMENTS

The Radiation Effects Research Foundation (RERF), Hiroshima and Nagasaki, Japan, is a private nonprofit foundation funded by the Japanese Ministry of Health, Labour and Welfare (MHLW) and the U.S. Department of Energy (DOE), with the latter provided through the U.S. National Academy of Sciences.

Received: January 21, 2004; accepted: February 20, 2004

REFERENCES

1. A. G. Knudson, Antioncogenes and human cancer. *Proc. Natl. Acad. Sci. USA* **90**, 10914–10921 (1993).
2. A. L. Jackson and L. A. Loeb, The contribution of endogenous sources of DNA damage to the multiple mutations in cancer. *Mutat. Res.* **477**, 7–21 (2001).
3. D. E. Thompson, K. Mabuchi, E. Ron, M. Soda, M. Tokunaga, S. Ochikubo, S. Sugimoto, T. Ikeda, M. Terasaki and S. Izumi, Cancer incidence in atomic bomb survivors. Part II: Solid tumors, 1958–1987. *Radiat. Res.* **137** (Suppl.), S17–S67 (1994).
4. J. S. Bedford and W. C. Dewey, Historical and current highlights in radiation biology: Has anything important been learned by irradiating cells? *Radiat. Res.* **158**, 251–291 (2002).
5. M. A. Kadhim, D. A. Macdonald, D. T. Goodhead, S. A. Lorimore, S. J. Marsden and E. G. Wright, Transmission of chromosomal instability after plutonium alpha-particle irradiation. *Nature* **355**, 738–740 (1992).
6. S. A. Lorimore, M. A. Kadhim, D. A. Pocock, D. Papworth, D. L. Stevens, D. T. Goodhead and E. G. Wright, Chromosomal instability in the descendants of unirradiated surviving cells after alpha-particle irradiation. *Proc. Natl. Acad. Sci. USA* **95**, 5730–5733 (1998).
7. J. B. Little, H. Nagasawa, T. Pfenning and H. Vetrovs, Radiation-induced genomic instability: Delayed mutagenic and cytogenetic effects of X rays and alpha particles. *Radiat. Res.* **148**, 299–307 (1997).
8. M. Shimizu, P. Gruz, H. Kamiya, S. R. Kim, F. M. Pisani, C. Ma-

sutani, Y. Kanke, H. Harashima and F. Hanaoka, Erroneous incorporation of oxidized DNA precursors by Y-family DNA polymerases. *EMBO Rep.* **4**, 269–273 (2003).

9. W. Yang, Damage repair DNA polymerases Y. *Curr. Opin. Struct. Biol.* **13**, 23–30 (2003).

10. S. M. Clutton, K. M. Townsend, C. Walker, J. D. Ansell and E. G. Wright, Radiation-induced genomic instability and persisting oxidative stress in primary bone marrow cultures. *Carcinogenesis* **17**, 1633–1639 (1996).

11. J. L. Redpath and M. Gutierrez, Kinetics of induction of reactive oxygen species during the post-irradiation expression of neoplastic transformation *in vitro*. *Int. J. Radiat. Biol.* **77**, 1081–1085 (2001).

12. R. E. Rugo, M. B. Secretan and R. H. Schiestl, X radiation causes a persistent induction of reactive oxygen species and a delayed reinduction of TP53 in normal human diploid fibroblasts. *Radiat. Res.* **158**, 210–219 (2002).

13. M. Muto, E. Kubo and T. Sado, Development of prelymphoma cells committed to thymic lymphomas during radiation-induced thymic lymphomagenesis in B10 mice. *Cancer Res.* **47**, 3469–3472 (1987).

14. H. Kawamoto, K. Ohmura, S. Fujimoto, M. Lu, T. Ikawa and Y. Katsura, Extensive proliferation of T cell lineage-restricted progenitors in the thymus: An essential process for clonal expression of diverse T cell receptor beta chains. *Eur. J. Immunol.* **33**, 606–615 (2003).

15. M. J. Bevan, In thymic selection, peptide diversity gives and takes away. *Immunity* **7**, 175–178 (1997).

16. G. Anderson, K. J. Hare and E. J. Jenkinson, Positive selection of thymocytes: The long and winding road. *Immunol. Today* **20**, 463–468 (1999).

17. J. Kumagai, K. Masui, Y. Itagaki, M. Shiotani, S. Kodama, M. Watanabe and T. Miyazaki, Long-lived mutagenic radicals induced in mammalian cells by ionizing radiation are mainly localized to proteins. *Radiat. Res.* **160**, 95–102 (2003).

18. J. K. Leach, G. Van Tuyle, P. S. Lin, R. Schmidt-Ullrich and R. B. Mikkelsen, Ionizing radiation-induced, mitochondria-dependent generation of reactive oxygen/nitrogen. *Cancer Res.* **61**, 3894–3901 (2001).

19. K. Polyak, Y. Xia, J. L. Zweier, K. W. Kinzler and B. Vogelstein, A model for p53-induced apoptosis. *Nature* **389**, 300–305 (1997).

20. G. Kroemer, N. Zamzami and S. A. Susin, Mitochondrial control of apoptosis. *Immunol. Today* **18**, 44–51 (1997).

21. C. L. Limoli, E. Giedzinski, W. F. Morgan, S. G. Swarts, G. D. Jones and W. Hyun, Persistent oxidative stress in chromosomally unstable cells. *Cancer Res.* **63**, 3107–3111 (2003).

22. S. DiMauro and E. A. Schon, Mitochondrial respiratory-chain diseases. *N. Engl. J. Med.* **348**, 2656–2668 (2003).

23. I. N. Zelko, T. J. Mariani and R. J. Folz, Superoxide dismutase multigene family: A comparison of the CuZn-SOD (SOD1), Mn-SOD (SOD2), and EC-SOD (SOD3) gene structures, evolution, and expression. *Free Radic. Biol. Med.* **33**, 337–349 (2002).

24. H. C. Lee and Y. H. Wei, Mitochondrial alterations, cellular response to oxidative stress and defective degradation of proteins in aging. *Biogerontology* **2**, 231–244 (2001).

25. Y. H. Wei, C. F. Lee, H. C. Lee, Y. S. Ma, C. W. Wang, C. Y. Lu and C. Y. Pang, Increases of mitochondrial mass and mitochondrial genome in association with enhanced oxidative stress in human cells harboring 4,977 BP-deleted mitochondrial DNA. *Ann. NY Acad. Sci.* **928**, 97–112 (2001).